



GLOBAL JOURNAL OF RESEARCHES IN ENGINEERING: A
MECHANICAL AND MECHANICS ENGINEERING
Volume 19 Issue 4 Version 1.0 Year 2019
Type: Double Blind Peer Reviewed International Research Journal
Publisher: Global Journals
Online ISSN: 2249-4596 & Print ISSN: 0975-5861

Refractory grade Bauxite: An Overview about the Effects of Different Bauxite Sources and Forming Processes on the Quality of the Material

By Vitor Guilherme de Oliveira, Luís Leonardo Horne Curimbaba Ferreira, Marcos Antônio dos Reis, Peter Miura Nakachima & André Luis Pereira

Abstract- Refractories have been very important for humankind development enabling the manufacturing of a wide range of materials. Primary industries demanding refractories include the manufacturing of steel, non-ferrous metals, glass, lime, cement, ceramics, petrochemicals and incineration. Refractory grade bauxites (RGBs) are high-alumina materials used as aggregates in shaped and unshaped refractory linings suitable to withstand high temperature heating and a corrosive environment. Despite the wide availability of bauxite ores in the world, few countries can supply a bauxite with refractory grades. Guyana, China and Brazil have emerged as suppliers for the refractory industry and the peculiarities of each bauxite from these countries impact directly on the refractory performance.

Keywords: refractory grade bauxite (RGB), high-alumina refractory, forming process.

GJRE-A Classification: FOR Code: 091399



Strictly as per the compliance and regulations of:



© 2019. Vitor Guilherme de Oliveira, Luís Leonardo Horne Curimbaba Ferreira, Marcos Antônio dos Reis, Peter Miura Nakachima & André Luis Pereira. This is a research/review paper, distributed under the terms of the Creative Commons Attribution-Noncommercial 3.0 Unported License <http://creativecommons.org/licenses/by-nc/3.0/>), permitting all non commercial use, distribution, and reproduction in any medium, provided the original work is properly cited.

Refractory grade Bauxite: An Overview about the Effects of Different Bauxite Sources and Forming Processes on the Quality of the Material

Vitor Guilherme de Oliveira ^α, Luís Leonardo Horne Curimbaba Ferreira ^σ, Marcos Antônio dos Reis ^ρ, Peter Miura Nakachima ^ω & André Luis Pereira ^ϕ

Abstract- Refractories have been very important for humankind development enabling the manufacturing of a wide range of materials. Primary industries demanding refractories include the manufacturing of steel, non-ferrous metals, glass, lime, cement, ceramics, petrochemicals and incineration. Refractory grade bauxites (RGBs) are high-alumina materials used as aggregates in shaped and unshaped refractory linings suitable to withstand high temperature heating and a corrosive environment. Despite the wide availability of bauxite ores in the world, few countries can supply a bauxite with refractory grades. Guyana, China and Brazil have emerged as suppliers for the refractory industry and the peculiarities of each bauxite from these countries impact directly on the refractory performance. This work aims to study different sources of RGB and how the manufacturing process can impact the refractory properties. The Guyanese RGB presented the highest alumina content (~90% Al₂O₃). However, a Brazilian RGB with lower alumina content (~85% Al₂O₃) presented the highest hot modulus of rupture value (HMoR at 1200°C/5h = 5.12 MPa). As for the Chinese RGBs, these presented a higher heterogeneity, evidenced in variation on chemical composition resulting in worse thermo mechanical performance (HMoR < 4.10 MPa). Two different forming process for Brazilian RGBs showed that the briquetting operation produces angular-shaped grains (sphericity = 0.7), whereas the extrusion mechanism produces rounded grains (sphericity = 0.9) which induce better flowability in castables.

Keywords: refractory grade bauxite (RGB), high-alumina refractory, forming process.

1. INTRODUCTION

Ceramic industry is an important global segment of the economy with several applications. There are different properties in ceramic materials that characterize their use and one of them is the refractoriness. A refractory material has the property of resisting the heat, the mechanical stress and/or chemical attacks, it means, not abrupt changes in its

chemical and physical properties in a wide temperature range and hostile environments, being a great raw material for applications in heat-processing industries as glass and metal industries [1].

The correct way of classifying a refractory must consider the sum of different factors. Regarding chemical composition, there are several names found in the refractory market: siliceous; silica-alumina; high-alumina; magnesian; chromitic-magnesian; chromic; graphite; zirconia-magnesia; and silicon carbide refractories; among several others. Formerly, the refractories are classified in acidic, basic, neutral or special by their chemical content and suitable environment of application, however it is not so useful nowadays due to the raw material combination in the refractory formulation. As for the shape, the refractory can be divided into shaped (bricks and cast shapes) and unshaped (monolithics), and it can still be classified as porous or dense according to the porosity level [2].

During the formulation of a refractory, close attention must be given to the selection of the refractory aggregate and the bonding system. Thus, refractories used in an iron-making process will differ from that of a steel-making process, since the nature of the metal and slag is different in these cases. In iron making, the metal and liquid slag are primarily neutral or slightly acidic in nature, whereas the slag is distinctively basic in the steel-making process. In summary, refractories chosen for iron making are based on alumina and silica, whereas magnesia-based refractories are the choice for steel making, because of their acidity and basicity, respectively [3][4].

Generally, the high-alumina refractories are marketed in terms of alumina content in intervals of 10%, ranging from 50% to higher than 90% [5]. According to the alumina content, Table 1 shows the possible raw materials and final predominant mineralogy of the refractory.

Author α ρ ω ϕ: Mineração Curimbaba Ltda. Rodovia Poços de Caldas / Caldas, km 10, Poços de Caldas – MG, Brazil.
e-mail: vitor.oliveira@curimbaba.com.br

Author α: Universidade Federal de Alfenas – UNIFAL Rodovia José Aurélio Vilela, 11.999, Poços de Caldas - MG, Brazil

Author σ ω ϕ: Elfusa Geral de Eletrofusão Ltda. Rua Júlio Michelazzo, 501, São João da Boa Vista – SP, Brazil.
e-mail: andre.pereira@curimbaba.com.br

Table 1: Different classes of high-alumina refractories (Adapted from [4]).

Alumina content	Raw material	Mineralogy predominant of refractory
50%	Fireclay	Mullite, glass/free silica
50%-60%	Alumina minerals & fireclay; bauxite and clay	Mullite, glass and free silica
70%	Bauxitic clay; calcined bauxite and clay	Mullite, corundum and glass
80%-85%	Calcined bauxite	Corundum, mullite and glass.
Above 90%	Tabular or fused alumina aggregates	Corundum, mullite and glass.

For this class of refractories, the alumina-silica phase equilibrium diagram, shown in Figure 1, can explain much of the mineralogy of the final product after sintering [4]. However, some impurities such as iron oxide, titanium oxide and alkalis react in high temperatures and can form other phases not shown in this diagram, as tialite, rutile and hematite. These impurities come from the raw materials used to make the refractory and it is in accordance with the mineralogy of the resources [5].

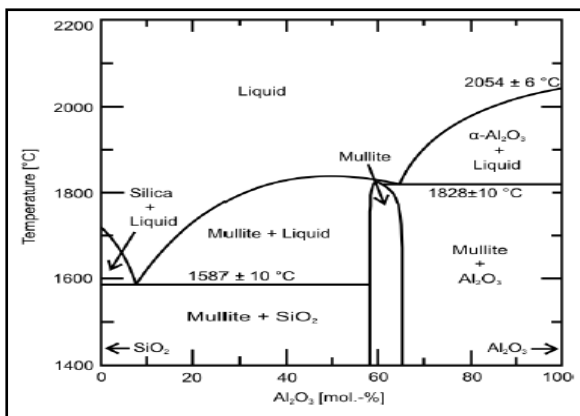


Figure 1: Silica-alumina phase-diagram.

As a note on phase equilibria diagram, refractories are usually not at thermo chemical equilibrium and the commercial refractories present some impurities. This means non-equilibrium phases may be present. An example might be a fireclay brick containing calcined bauxite aggregate (added for composition adjustment) with an overall composition of 50% Al_2O_3 . This fired brick will contain corundum even though the phase diagram says it should not be present [4].

Globally, above 85% of the processed bauxite is destined to alumina production through Bayer Process and 94% of all this alumina is processed by Hall-Héroult process, to turn alumina to metal aluminum [2][6][7]. The remaining bauxite, or non-metallurgical bauxite, is destined for some other segments. Among them, it is inserted the refractory products, which iron and steelmakers consume more than 70% of the world production [6].

Guyana pioneered the manufacturing of RGB since 1940's. China began supplying only in the 1970's. Afterwards, Brazil started to produce some quantities [8]. According to the Ministry of Natural Resources of Guyana [6], 1.88 Mt of worldwide bauxite were directed to RGB production in 2015, being the main consumers China, Russia and India, existing only two significant worldwide suppliers: China and Guyana. According to the same source, Guyana was responsible for 6.6% of world's RGB supply in 2015, while China takes the remainder. These numbers are close to the ones published by other sources, showing China currently with 95% of the world market share [9][10].

While bauxite ore from Brazil, Guyana and other areas with tropical climate tends to be gibbsitic ($Al(OH)_3$) whose aluminum hydroxide is trihydrate, Chinese one is mainly diasporic ($\alpha-AlO(OH)$), a monohydrate [11]. In general, bauxite ores from these countries exhibit different mineralogy and physicochemical characteristics that promote different properties on the RGBs manufactured [12]. Traditionally, the mineralogy of RGB is composed by a combination among three or more phases, hereinafter referred: corundum (1st phase), mullite (2nd phase), tialite, rutile and/or hematite. Table 2 shows some properties of each phase mentioned [13][14][15][16][17].

Table 2: Properties of RGB mineralogical phases

Phase	Corundum	Mullite	Tialite	Hematite	Rutile
Melting Temperature (°C)	2050	1828	1860	1595	1668
Density (g/cm ³)	4.0	3.2	3.7	5.2	4.5

Thermal Conductivity (W/m.K)	33	3.9-6.3	1.5-2.5	7.85-9.03	7.4
Thermal Expansion ($\times 10^{-6} K^{-1}$)	4.6	α_a 3.1-4.1	α_a 11.8	11.8	8.5-9.5
		α_b 5.6-7.0	α_b 19.4		
		α_c 5.6-6.1	α_c (-2.6)		

Considering thermal process, the diasporite from raw bauxite is straightly converted to α -alumina during the firing, without metastable transition alumina [18], assuring the crystal growth and inhibiting the reaction with silica in the liquid phase to form mullite [12]. Furthermore, the higher grade of titanium oxide in Chinese bauxite favors the tialite formation (β - $Al_2O_3 \cdot TiO_2$) above 1350°C which can be an issue considering the mechanical strength due to its highly anisotropic thermal expansion (Table 2) and an eutectoid transformation during the cooling, decomposing it into its precursors, alumina and titania, in a wide range of intermediate temperature (750°C –1300°C) [14]. When gibbsite is the main mineral as per Brazilian and Guyanese bauxites, there are many phase transformations until corundum formation [18]. The slower grain growth facilitates the reaction between alumina and silica, increasing the mullite amount in the final product.

Recently, a Brazilian RGB produced with a gibbsitic bauxite was characterized and presented 19.4% (by weight) in mullite (acicular-shaped), while a Chinese RGB produced with a diasporic bauxite showed 15.4% in mullite (not acicular-shaped) and 4.4% in tialite (small crystallites). Bricks made with these RGBs using a conventional castable formulation showed the impact of those mineralogies in the thermo mechanical behavior, where the bricks made with Brazilian RGB withstood the hot load test (25 psi at 1600°C) and the bricks made with Chinese RGB failed under the same conditions [12].

Another work compared the difference between two processing ways of calcined bauxite: calcining from run of mine (ROM) bauxite, and calcining a bauxite after an ore processing, composed of size reduction, mixing

and agglomeration. Processed bauxite showed the best results in the stress-strain test conducted under compression load in air. Moreover, the grains spatial distribution was remarkably more homogenous, demonstrating the importance of the processing in the final product properties and performance [19].

In a study which the aim was comparing four different forming processes (uniaxial pressing, extruding, lamination and slip casting) on sintered clay properties, the highest densification in the green body was obtained by pressing technique and it promoted larger quantity of mullite [20]. Japanese researchers studying forming processes of a porous ceramic (SiC) showed that compression molding (or uniaxial pressing) led to higher strength and homogeneity of the ceramic matrix, while extrusion led to lower strength and higher apparent porosity [21].

In an industrial scale, there are different technologies employed for the forming operations like briquetting or extrusion. Briquetting is a technique for agglomeration of fine particles under stresses like compression. The briquetting can be performed by a roller press (or briquette machine), in which a pressure is used to shape the material through its molds in the rolls surface. In this machine, the feedstock is forced to pass between two rolls that will produce the geometrical form of the material [22]. As for the industrial extruders, these can be manufactured with a single-screw, twin-screw or piston. The feed of this equipment needs to be done with a material having an optimum level of plasticity and flowability. The equipment, by screw rotation or piston pushing, will shape the product according its nozzle or die. Figure 2 shows a diagram for both equipment.

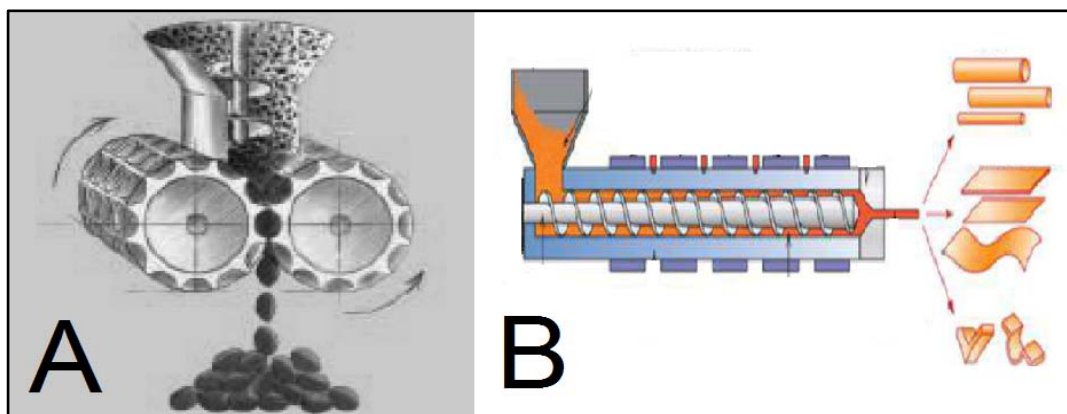


Figure 2: Diagram of forming machines: (A) briquette machine; (B) extruder (Adapted from [22] and [23]).

To improve the quality of briquettes, organic binders can be added to the raw materials before the forming process. Outstanding results were found by adding low percentages of corn starch or lignosulfonates into refractory grade bauxites, increasing the resistance of the green bodies formed [24].

In this work, the authors present a comparison between the technical properties of different refractory grade bauxites from China, Guyana and Brazil. For the case of Chinese RGBs, two classes were evaluated according to their alumina content (86% Al_2O_3 and 88%

Al_2O_3). For Brazilian RGBs, two forming process were taken into account (extrusion and briquetting).

II. MATERIALS AND METHODS

Five samples of RGB in four size fractions as described in Table 3 were selected for this work: two Brazilian ones (MC A and MC B), one from Guyana (G) and two from China (CH86 and CH88). Figure 3 shows the samples and their size fractions.

Table 3: Description of the RGB fractions

Size Fractions	Description
-6.70 +2.36 mm	Particles predominantly smaller than 6.70 mm (opening diameter of a sieve = 0.265") and larger than 2.36 mm (8 mesh).
-2.36 +0.85 mm	Particles predominantly smaller than 2.36 mm (8 mesh) and larger than 0.85 mm (20 mesh).
-0.85 mm	Particles predominantly smaller than 0.85 mm (20 mesh).
-0.075 mm	Particles predominantly finer than 0.075 mm (200 mesh).





















RGB	-6.70 +2.36 mm	-2.36 +0.85 mm	-0.85 mm	-0.075 mm
MC A (Brazilian)				
MC B (Brazilian)				
G (Guyanese)				
CH86 (Chinese)				
CH88 (Chinese)				

Figure 3: RGB samples and their size fractions

For Brazilian RGBs, the processing sequence began with a selection of bauxite ores as raw materials for an initial blending. The chemical composition for the crude bauxite blend was checked aiming to achieve an iron oxide (Fe_2O_3) content lower than 3.5% and a titanium oxide (TiO_2) content lower than 1.0%. Additionally, a special attention is taken to ensure the

low alkaline oxides content. Such analysis result by X-Ray Fluorescence Spectrometry is shown in Table 4.

Afterwards, the right bauxite blend was dried and the material went through homogenization, milling and water addition for adjusting the moisture, until achieve an optimum plasticity to assure the forming processes.

Table 4: Chemical composition (%wt.) of the Brazilian bauxite blend (dry basis)

Al ₂ O ₃	SiO ₂	Fe ₂ O ₃	TiO ₂	K ₂ O	RO*	LOI**
59.0	5.03	3.29	0.75	0.06	0.09	31.5
*RO = CaO + MgO						
**LOI = Loss on ignition at 1100°C/2h						

Regarding the forming processes, two different routes were considered. MC A was produced using a single-screw-extruder and MC B was manufactured with a briquette machine. After conformation, MC B went

through a lump crusher to reduce the size of the briquettes and, only after this crushing, the material was transferred to a rotary kiln for sintering. As for MC A route, the extruded material was straightly directed to a rotary kiln, eliminating the physical comminution step. Both materials were sintered over 1700 °C, and the run of kiln product was cooled through a rotary cooler and sized into the fractions “-6.70|+2.36 mm”, “-2.36|+0.85 mm” and “-0.85 mm” by vibratory screening. Lastly, the fraction “-0.075 mm” was obtained by ball milling. Figure 4 presents a concise flowchart of the Brazilian RGB with its two forming processing routes.

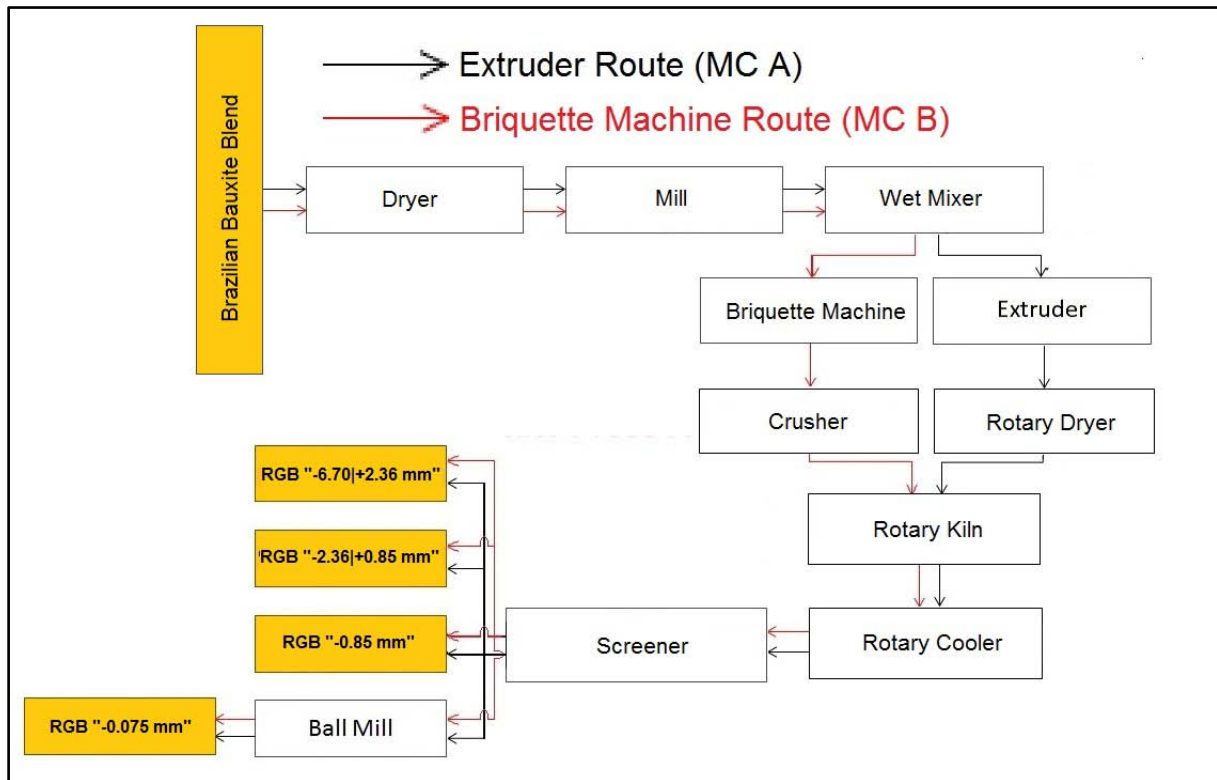


Figure 4: Flowchart for Brazilian RGB production using a single-screw-extruder or a roller press (briquette machine)

All RGBs were analyzed for particle-size distribution (PSD) in terms of retained weight on ASTM Standard sieves, and the “-6.70|+2.36 mm”, “-2.36|+0.85 mm” and “-0.85 mm” size range should also have their particles shape evaluated in terms of sphericity. The sieves used for each size range are listed in Table 5 and the pattern for visual estimation of sphericity based on Krumbein Index is presented in Figure 5. Particularly for the fraction “-0.075 mm”, due to their fineness, the PSD of the samples in terms of volume were obtained by laser diffraction (Malvern Mastersizer 2000).

Table 5: Sieves used for the particle-size analysis.

Size Range	Sieves ASTM Standard Number (and opening diameter in millimeter)				
	0.265" (6.70)	#4 (4.75)	#6 (3.35)	#8 (2.36)	#10 (2.00)
-6.70 +2.36 mm					
-2.36 +0.85 mm	#6 (3.35)	#10 (2.00)	#18 (1.00)	#20 (0.85)	
-0.85 mm	#16 (1.18)	#18 (1.00)	#20 (0.85)	#30 (0.60)	

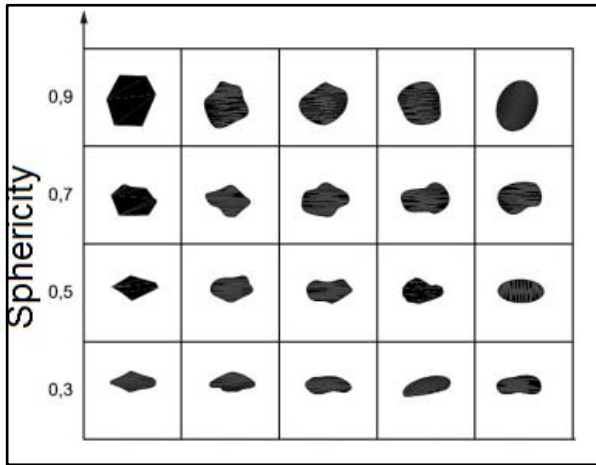


Figure 5: Chart for visual reference of particle sphericity (adapted from [25]).

All the samples were chemically analyzed by X ray fluorescence technique in a sequential wavelength dispersive spectrometer (XRF 1800, Shimadzu) after sample preparation by fusion method in a high frequency induction machine (HA-HF 16/2, Herzog).

The RGB mineralogy for the “-6.70|+2.36 mm” size range was evaluated by X-ray diffractometry in a vertical θ -2 θ diffractometer (XRD 6000, Shimadzu), operating with a source of $\text{CuK}\alpha$ radiation (power = 40 kV, 30 mA) in a step scan mode (step = 0.02° 2 θ , time = 2 s, scan range = 15 to 80° 2 θ). After mineralogical phases identification, the Rietveld method was applied for quantitative phases analysis [26][27].

The apparent porosity, water absorption and specific gravity of the solid fraction for “-6.70|+2.36 mm” samples were evaluated through the Archimedes Principle by hot water intrusion pycnometry [28]. For the remaining fractions, the specific gravity was obtained as real density by helium gas intrusion pycnometry.

Performance tests were conducted in a convention castable formulation with 82% aggregates (RGBs) and 18% high-purity calcium aluminate cement (HP-CAC). For this test, a pre-mix of different sizes of RGB was prepared according to the following composition: 30%wt. “-6.70|+2.36 mm”; 30%wt. “-2.36|+0.85 mm”; 30%wt. “-0.85 mm”; 10%wt. “-0.075 mm”. The PSD and the chemical composition of the HP-CAC are presented in Figure 6 and Table 6, respectively.

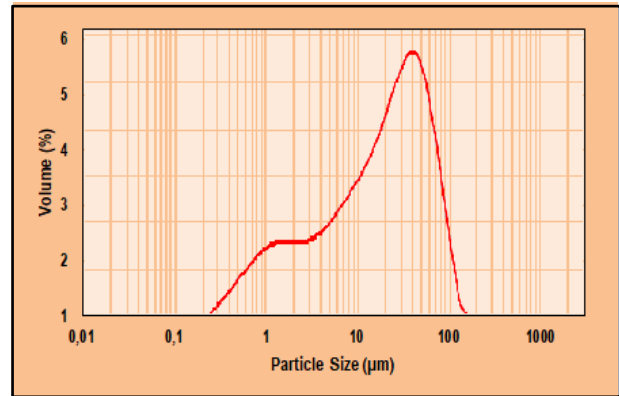


Figure 6: Particle size distribution of the HP-CAC

Table 6: Chemical composition (%wt.) of the HP-CAC

Al_2O_3	CaO	SiO_2	Fe_2O_3	TiO_2	K_2O	Na_2O
69.5	24.3	3.23	2.31	0.24	0.16	0.04

The castables were prepared with a water to concrete ratio in 9%wt. After 24 hours of curing time at room temperature, the castables were dried in a stove for 24 hours/ 110°C . The determination of the hot modulus of rupture (HMoR) was performed at 1200°C after five-hour of soaking time using the three-point bending technique [29]. The workability of the castables was also evaluated, and the phase identifications for the fired concretes were performed by X-ray diffractometry, aiming to evaluate the new phases formation under firing.

Flowability tests [30] were performed for the castables with Brazilian RGBs as aggregate (MC A and MC B), aiming to evaluate the morphology effect on it. In this special case, the aggregates fraction used was the “-6.70|+2.36 mm” size only.

III. RESULTS AND DISCUSSION

The chemical composition for each RGB size is presented in Table 7. The RGB G samples presented the highest aluminum oxide content on average ($\sim 90\%$), followed by CH88 ($\sim 87\%$), CH86 ($\sim 86\%$), MC A ($\sim 85\%$) and MC B (85%). The impurities varied with the samples, where Brazilian RGBs showed a considerable content of iron oxide (4-5%) and a low content of titanium, the Guyanese and Chinese RGBs showed a high content of titanium oxide (3-4%). These impurities can promote the formation of deleterious phases for refractories, specially tialite formation due to titanium presence.

Table 7: Chemical composition (%wt.) for the fractions of RGBs

RGB	Size Range	Al ₂ O ₃	SiO ₂	Fe ₂ O ₃	TiO ₂	K ₂ O	RO*
MCA	-6.70 +2.36 mm	85.2	8.18	4.80	1.20	0.15	0.17
	-2.36 +0.85 mm	85.4	8.04	4.81	1.20	0.13	0.14
	-0.85 mm	85.2	8.26	4.67	1.27	0.13	0.13
	-0.075 mm	84.5	8.22	5.20	1.33	0.08	0.30
MCB	-6.70 +2.36 mm	86.1	7.37	4.70	1.19	0.12	0.18
	-2.36 +0.85 mm	85.0	8.06	5.06	1.26	0.10	0.16
	-0.85 mm	83.5	10.1	4.60	1.06	0.14	0.27
	-0.075 mm	85.1	7.81	5.15	1.28	0.08	0.24
G	-6.70 +2.36 mm	89.2	6.02	1.24	2.97	0.00	0.10
	-2.36 +0.85 mm	90.3	5.17	1.26	2.81	0.00	0.04
	-0.85 mm	90.0	5.17	1.33	3.04	0.00	0.02
	-0.075 mm	89.4	5.48	1.67	2.93	0.00	0.04
CH86	-6.70 +2.36 mm	86.9	7.05	1.37	3.49	0.14	0.44
	-2.36 +0.85 mm	87.9	6.05	1.27	3.33	0.26	0.59
	-0.85 mm	84.9	8.39	1.97	3.27	0.17	0.70
	-0.075 mm	85.5	8.11	1.50	3.28	0.33	0.61
CH88	-6.70 +2.36 mm	88.3	5.77	1.22	3.32	0.25	0.49
	-2.36 +0.85 mm	89.0	5.27	1.10	3.27	0.27	0.48
	-0.85 mm	85.8	8.19	1.36	3.48	0.19	0.36
	-0.075 mm	85.2	8.31	1.39	3.67	0.15	0.62

*RO: CaO + MgO.

The silica content decreased with the increasing of the particle size for Chinese RGBs. For instance, in the RGB CH88, silica content was 8.31% in the fraction "-0.075 mm", whereas for the fraction "-2.36|+0.85 mm", the lowest result was encountered (5.27%).

The higher content of alkalis and earth-alkaline oxides (K₂O and RO in Table 7) can configure another source of concerns for Chinese RGBs, because these oxides are related to the lowering of the softening point of the material.

Table 8 shows a statistic treatment considering the variation on chemical composition of the RGBs. The highest standard deviations were also encountered for

the Chinese RGBs, mainly for the silica content. RGB MC A has the most homogeneous chemical composition. For MC A route, the feeding of the extruder demands a finer milling, ensuring a more effective mixture and preventing a chemical segregation during the process. The processes of milling, mixing and agglomerating work against the natural heterogeneity of the mineral resources of bauxite. Heterogeneity is connected with the aspect of the aggregate, in which the Chinese ones are colorful (i.e. singular grains in black, grey and brown), denoting a chemical and mineralogical heterogeneity.

Table 8: Standard deviation (%wt.) of main oxides of each RGB

RGB	Al ₂ O ₃	SiO ₂	Fe ₂ O ₃	TiO ₂	K ₂ O	RO*	Sum
MC A	0.39	0.10	0.23	0.06	0.03	0.08	0.89
MC B	1.07	1.21	0.27	0.10	0.03	0.05	2.73
G	0.51	0.40	0.20	0.10	0.00	0.03	1.24
CH86	1.36	1.07	0.31	0.10	0.09	0.11	3.03
CH88	1.86	1.59	0.13	0.18	0.06	0.11	3.92

*RO: CaO + MgO.

The diffractogram and mineralogical composition of the RGBs are presented in Figure 7 and Table 9, respectively. Chinese RGBs presented the highest content of corundum, while the Brazilian ones the lowest. Corundum is the major phase of the calcined

bauxites, and the most refractory phase in high-alumina refractories (Table 2).

Brazilian RGBs contain hematite in a low content, what can reduce the refractoriness of the system (Table 2). Both Guyanese and Chinese RGBs

presented tialite, but only the Chinese RGBs showed a small quantity of rutile, due to a eutectoid reaction of decomposition of tialite and/or lack of energy, temperature or homogenization for the reaction of all the titanium oxide with the aluminum oxide. The tialite phase brings some concerns because its formation is not irreversible and the refractory integrity can be impaired due to its highly anisotropic thermal expansion (Table 2).

Mullite is the secondary phase for all RGBs, having the greatest amounts for RGB MC A (20%) and RGB G (19%). The highest alumina content in RGB G (~89%) suggests a mullite richer in alumina ($3Al_2O_3 \cdot 2SiO_2$ to $2Al_2O_3 \cdot 1SiO_2$, Fig. 1). This higher grade of alumina in the stoichiometry of the mullite is caused by a substitution of a Si^{4+} cation and a removal of an oxygen ion from a $(Al,Si)O_4$ tetrahedron in its crystal structure, enriching the alumina content [13].

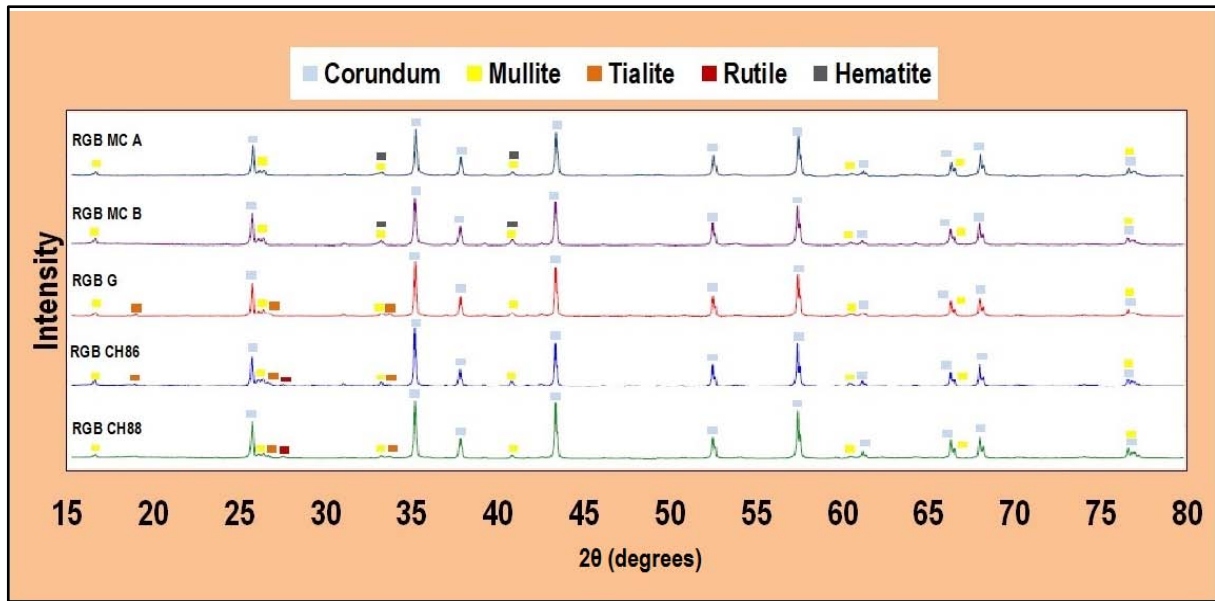


Figure 7: X-ray diffractograms for RGBs in the “-6.70|+2.36” mm fractions

Table 9: Mineralogical Composition (%wt.) for RGBs in the “-6.70|+2.36” mm fractions

Phase	Chemical Formula	MC A	MC B	G	CH86	CH88
Corundum	Al_2O_3	76.4	80.5	75.7	76.6	90.0
Mullite	$Al_{4+2x}Si_{2-2x}O_{10-x}$	20.0	16.6	19.0	16.9	5.20
Tialite	Al_2TiO_5	-	-	5.30	5.70	4.20
Rutile	TiO_2	-	-	-	0.80	0.60
Hematite	Fe_2O_3	3.60	2.90	-	-	-

Figure 8 shows the particle size distribution (PSD) for all the RGBs studied in this work. In general, the samples were within the size range specified (at least 80%wt. of the particles between the reference screens). Regarding the fraction “-6.70|+2.36 mm”, Brazilian RGBs diverged from the other bauxites, presenting a higher quantity for finer particles, and a wider curve with maximum retention on sieve 2.36 mm. Chinese and Guyanese RGBs had a narrower distribution and the maximum retention on sieve 3.35 mm. For fraction “-2.36|+0.85 mm” the opposite occurred, the Brazilian RGBs had a narrower distribution, but continuing finer than the other bauxites.

Comparing the forming processes (MC A x MC B), Brazilian RGBs presented the same behavior about the size distribution for all fractions, except for “-0.85 mm” samples, where MC A sample had 70%wt. of retention on 0.60 mm opening screen, in comparison with the other samples which had more than 70%wt. of the particles passing by that same screen. It’s remarkable the influence of the forming process on the particle size, being the extrusion method responsible for the generation of a “-0.85mm” fraction with the most part of the particles distributed in -0.85 mm|+0.60 mm screens.

For “-0.075 mm” fractions analyzed by laser diffraction, the Brazilian RGBs showed the same

behavior and intensity due to the ball milling operation, common for all samples.

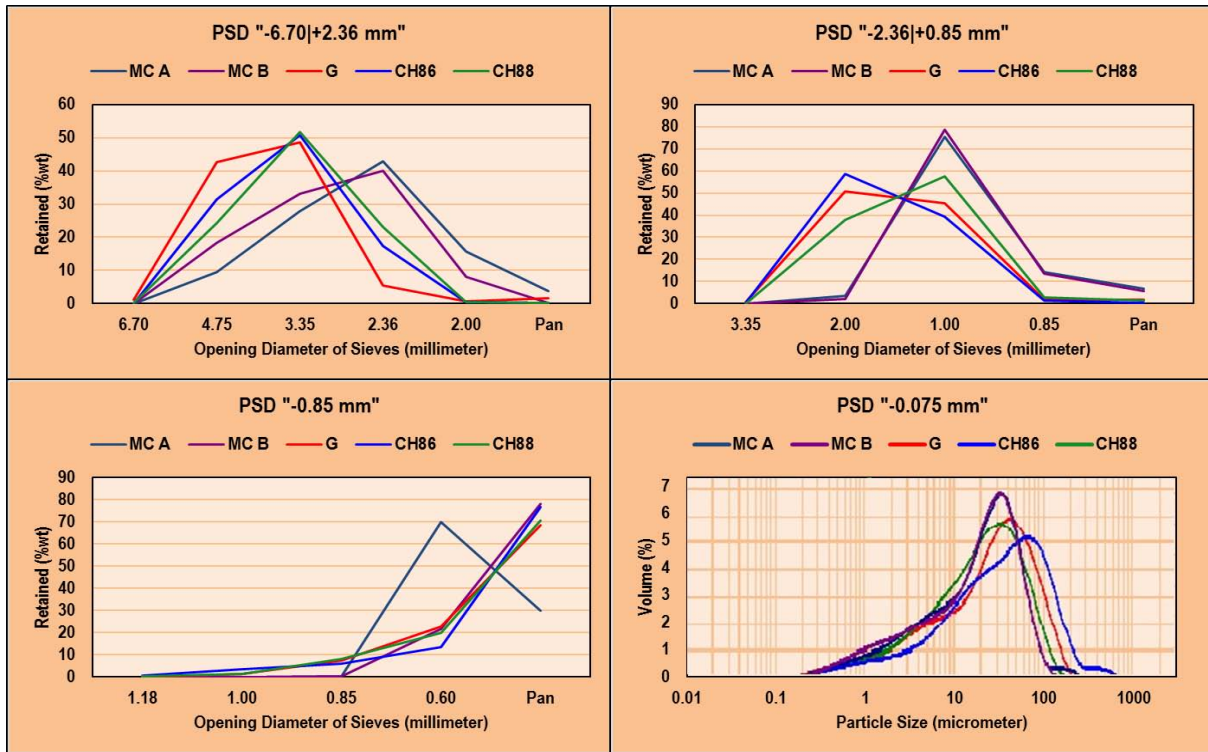


Figure 8: Particle size distributions of the RGB fractions

The sphericity of the three coarser fractions for all the RGB samples is presented by Table 10. The products from the extruder were rounded granules, while the briquette machine formed irregular-shaped particles, setting the main physical difference among

those samples. Depending on the type of application, rounded grains can facilitate pumping operations and reduce the power employed to transport the material. Likewise, spherical grains play in favor of self-flow.

Table 10: Sphericity of the RGBs in different size fractions: “-6.70 | +2.36 mm”; “-2.36 | +0.85 mm”; “-0.85 mm”

RGB	Sphericity			
	-6.70 +2.36 mm	-2.36 +0.85 mm	-0.85 mm	Average
MC A	0.8	0.9	0.9	0.9
MC B	0.6	0.7	0.7	0.7
G	0.5	0.6	0.6	0.6
CH86	0.6	0.5	0.6	0.6
CH88	0.6	0.5	0.6	0.6

Regarding the apparent porosity and water absorption, results for all RGBs are presented in Figure 9. Apparent porosity of the Chinese RGBs are the lowest, whereas for the Guyanese RGB is the highest. Despite the Guyanese RGB chemical composition is the richest in aluminum oxide, its high porosity can be detrimental to the mechanical performance of the refractory. The Brazilian RGBs have a high apparent porosity, however the RGB MC B is lower than RGB MC A due to a higher compression in the briquette machine,

if compared with an extruder. Water absorption is directly proportional to apparent porosity.

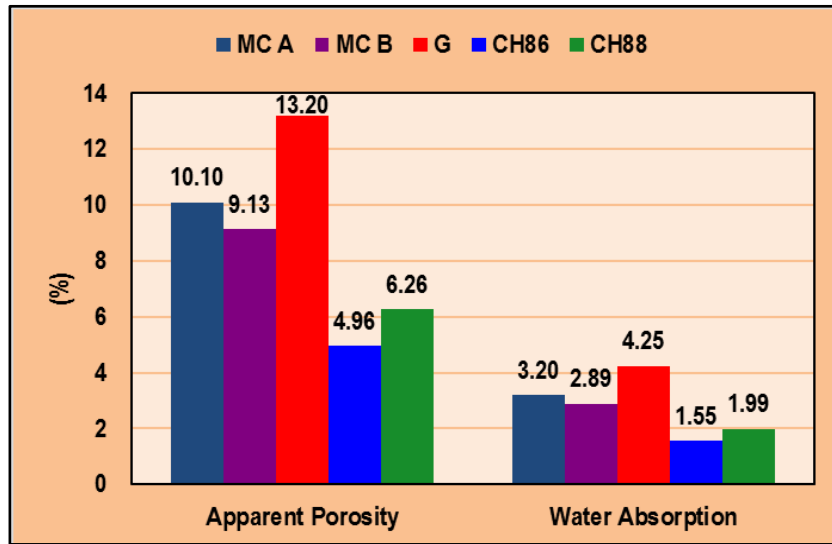


Figure 9: Physical indexes of RGBs in the "-6.70|+2.36" mm fraction

The specific gravities of all samples are presented in Figure 10. In general, the specific gravities increase with the decreasing of the particle sizes. It shows that, the reduction on number of closed pores in the particles, is proportional to the decreasing of the size of particles. That is, coarser particles have a higher number of closed pores, resulting in a lower weight per volume of material. The Guyanese RGB has the highest

values in this property, what is good for a refractory because specific gravity relates with mechanical performance. The Brazilian RGBs have a specific gravity higher than the Chinese ones for the "-6.70|+2.36 mm" fraction, but lower for the "-0.85 mm" one. It can be related to the firing conditions, since the materials are sintered during the same run of kiln.

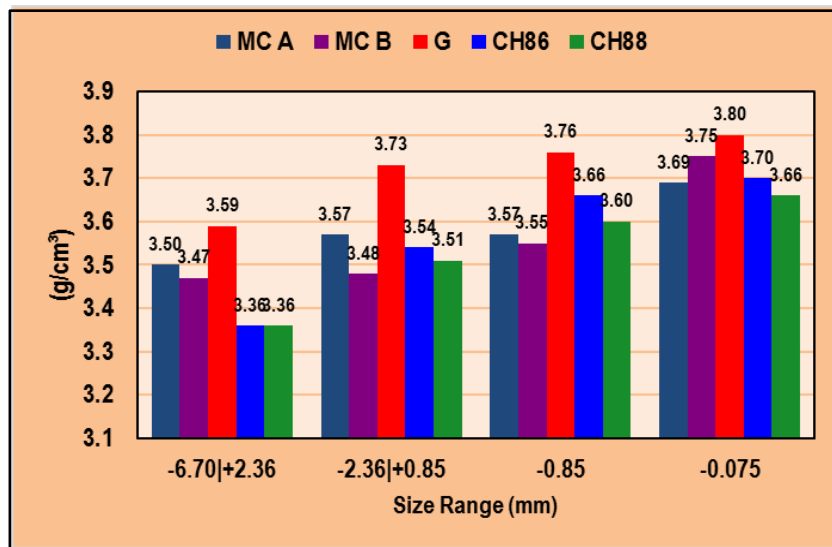


Figure 10: Specific gravity of the particles of RGB in each size range

The hot modulus of rupture (HMoR) at 1200°C of the castables measured through the three-point bending technique and the sum of the standard deviation on chemical composition (SDoCC) of the RGBs are shown in Figure 11. This performance test contemplates the effect of all properties discussed. In statistical terms, the results are in a same magnitude, being possible to infer that the crack propagation occurred through the cement matrix, and not throughout

the aggregate grains (Figure 12). However, there is a noticeable correlation between the HMoR and the SDoCC of RGBs. The lower the chemical variability (deviation sum), the higher the mechanical strength (HMoR). In absolute terms, RGB MC A presented the best flexure strength (5.12 MPa) and RGB G the second one (5.04 MPa). In spite of having 90% of corundum (Table 9), the heterogeneity of RGB CH88 aggregates may have been a decisive factor of its worst thermo

mechanical performance. Isolated grains rich in phases as talite or poorer in alumina can be harmful for refractory resistance. However, all the castables

presented a good workability and the working time achieved for each castable is shown in Figure 13.

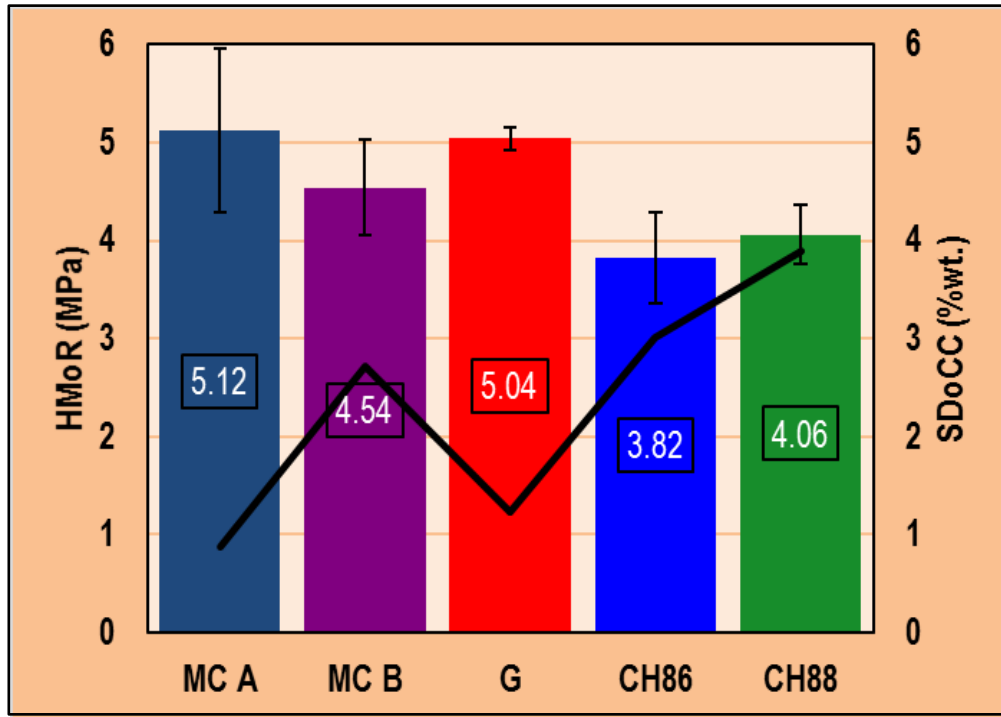


Figure 11: Hot modulus of rupture of castables produced with different RGB sources (column graph) and standard deviation on chemical composition of RGBs (line graph)

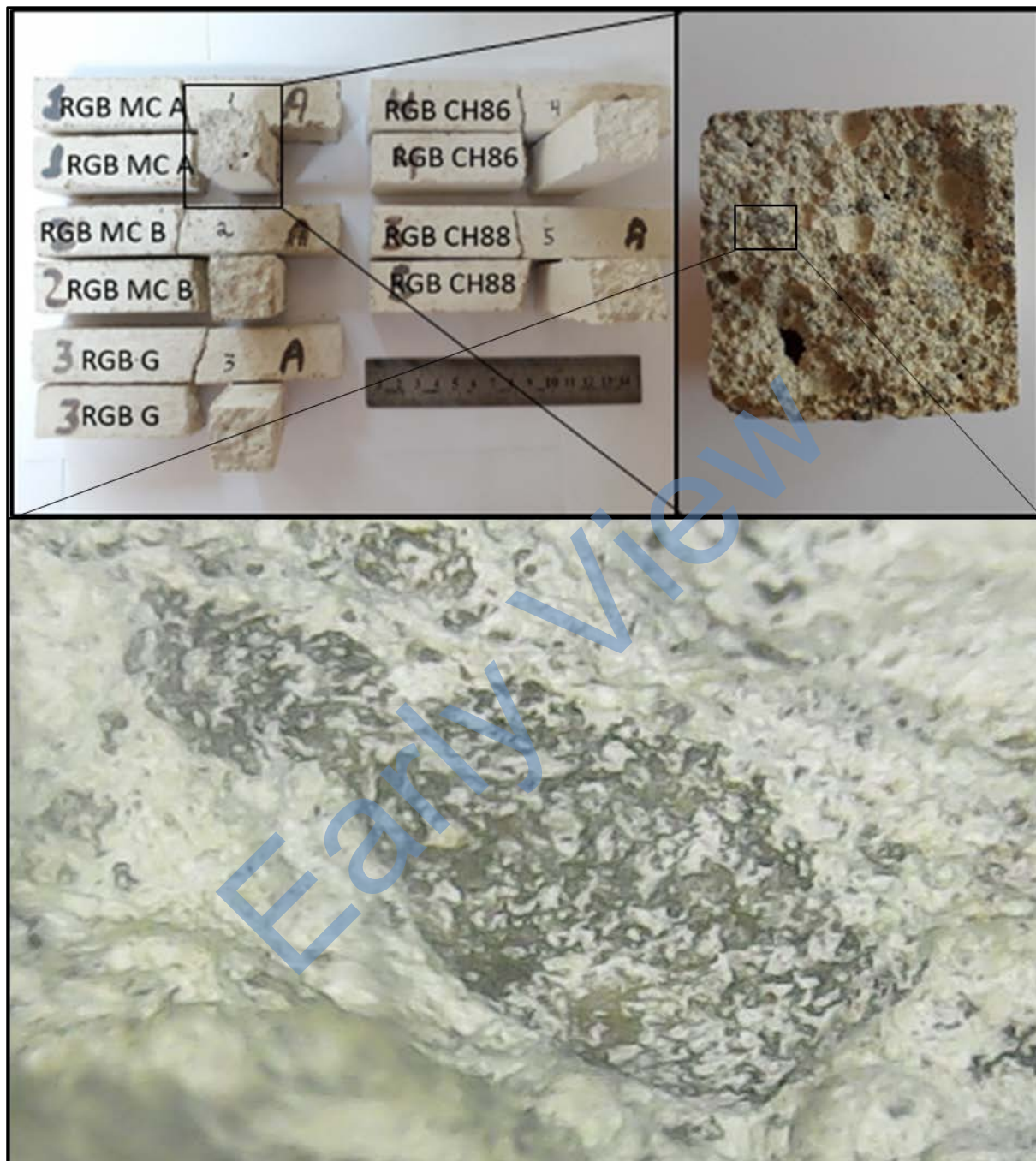


Figure 12: Specimens after hot modulus of rupture test, highlighting a good interaction between the RGB grain (sample MC A) and the cement matrix

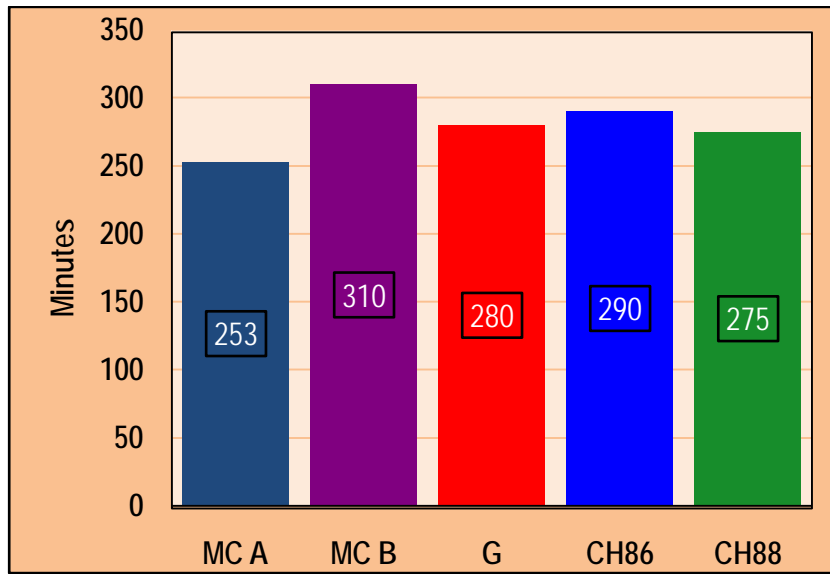


Figure 13: Workability of castables with RGBs as aggregate

Figure 14 shows the diffractograms of the castables after HMoR test, and the Table 11 lists the phases identified for each one, pointing them out in colored blocks. In addition to RGB phases, CAC phases such as grossite, gehlenite and hibonite were found.

Anorthite was found in all castables, result of a thermal reaction between the CAC binder and the RGB matrix. Especially for RGB G, a cristobalite peak was found, what can be related to silica crystallization from liquid phase cooling.

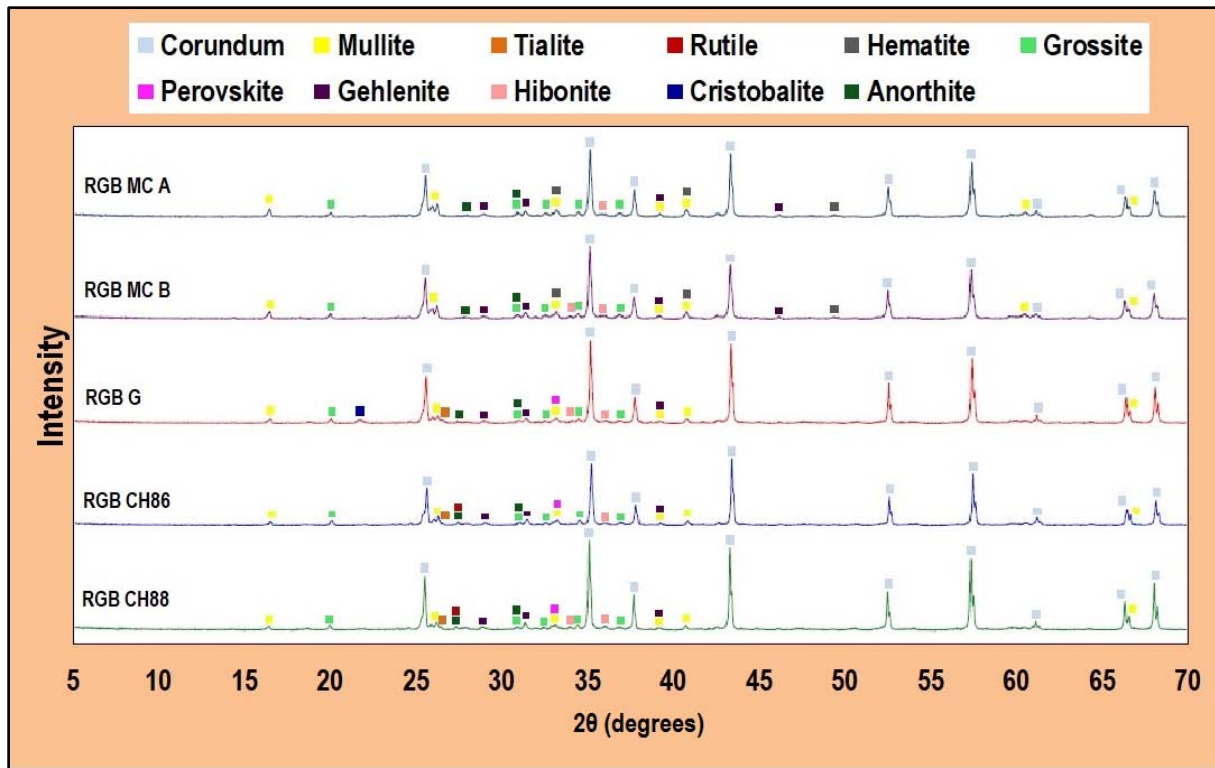


Figure 14: X-ray diffractograms of castables produced with different RGB sources and fired at 1200°C/5h

Table 11: Mineralogy of the castables after HMoR

Phase	MC A	MC B	G	CH86	CH88
Corundum (Al ₂ O ₃)					
Mullite (Al ₆ Si ₂ O ₁₃)					
Tialite (Al ₂ TiO ₅)	Not	Not			
Rutile (TiO ₂)	Not	Not	Not		
Hematite (Fe ₂ O ₃)			Not	Not	Not
Grossite (CaAl ₄ O ₇)					
Perovskite (CaTiO ₃)	Not	Not			
Gehlenite (Ca ₂ Al ₂ SiO ₇)					
Hibonite (CaAl ₁₂ O ₁₉)					
Cristobalite (SiO ₂)	Not	Not		Not	Not
Anorthite (CaAl ₂ Si ₂ O ₈)					

The flowability test of the castable varying the type of forming process for Brazilian RGBs showed the influence of particle morphology. The results are shown in Figure 15. The higher the displacement, the higher the flowability. The castable with RGB MC A as aggregate presented a higher flowability when compared to the

one with RGB MC B. Hence, being the particles rearrangement a function of the beats on the flow table, the more spherical-shaped particles in RGB MC A proportionated the higher displacement of the castable by rolling of those thick particles.

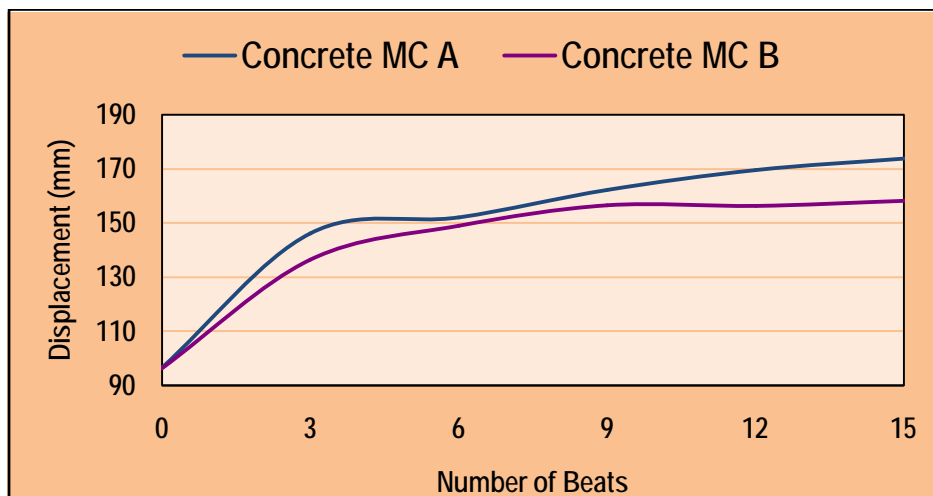


Figure 15: The impact of the forming process of RGBs on concretes flowability

IV. CONCLUSIONS

Refractory properties are a correlation between characteristics of raw material and the processing employed. Mineralogy, chemical composition, firing temperature, particle size, forming process and porosity index will define the performance of the refractory. Thermo mechanical tests presented a relationship with the variability of the chemical composition among the size fractions for the same RGB. The Brazilian RGB processed in an extruder (MC A), with the lowest standard variation on chemical composition (SDoCC = 0.88%) and tialite absence in its composition, promoted a castable with the highest hot modulus of rupture value (HMoR at 1200°C = 5.12 MPa). Guyanese RGB also got a great result (HMoR = 5.04 MPa), whereas the Chinese

RGBs were the least resistant (HMoR: CH86 = 3.82 MPa; CH88 = 4.06 MPa), in accordance with their higher heterogeneity represented by the standard deviation on chemical composition (SDoCC: CH86 = 3.03%; CH88 = 3.92%).

All the refractory grade bauxites presented a high aluminum oxide content (> 83%), corundum and mullite as main phases, and a suitable working time (over 250 minutes) in a conventional castable formulation.

Despite of the highest alumina content (~90% Al₂O₃) of the Guyanese RGB, it has exhibited the lowest corundum content (75.7%), what can be related to a formation of a mullite richer in alumina (19.0%). The Chinese sample "RGB CH88" presented the highest corundum content (90%), however their impurities

enabled tialite formation (4.20%) which may have impaired the high temperature strength. Brazilian RGBs (MC A and MC B) presented high mullite content (20.0% and 16.6%) and low hematite content (3.60% and 2.90%), in a good balance with corundum (76.4% and 80.5%), promoting highly homogeneous grains and proper physical indexes for refractory applications as dense granulated materials.

The size and the morphology of the RGBs is affected by the processing route, and the shape of the grains impacted the flowability. Two different forming process for Brazilian RGBs showed that the briquetting operation produced angular-shaped grains (MC B: sphericity = 0.7) due to a briquettes fragmentation, whereas the extrusion mechanism produced rounded grains (MC A: sphericity = 0.9) which induced the flowability of the castables, comparing the displacement of both castables (MC A x MC B) on a flow table.

REFERENCES RÉFÉRENCES REFERENCIAS

1. M. Allaby, Dictionary of Earth Sciences, New York: Oxford University Press Inc., 2008.
2. M. Victoria, "Argilas e Minerais Refratários," Companhia de Desenvolvimento de Minas Gerais, Belo Horizonte, 2018.
3. S. Banerjee, "Properties of Refractories," in Refractories Handbook, Boca Raton, Taylor & Francis Group, 2004.
4. D. A. Brosnan, "Alumina-Silica Brick," in Refractories Handbook, Boca Raton, Taylor & Francis Group, 2004.
5. Harbison-Walker Refractories Company, Handbook of Refractory Practice, Moon Township, 2005.
6. MRNG, "Bauxite Polite Briefs - Final Drafts," 10 July 2019. [Online]. Available: <https://nre.gov.gy/2019/07/18/bauxite-policy-briefs-final-drafts/>. [Accessed 19 September 2019].
7. USGS, "Bauxite and Alumina Statistics and Information," 2019. [Online]. Available: <https://minerals.usgs.gov/minerals/pubs/commodity/bauxite/>. [Accessed 19 September 2019].
8. S. Hinds, "Refractory Bauxites," IM Refractories Supplement, 1983.
9. R. Flook, "Refractory evolution - implications for bauxite & alumina," in 3rd Asian Bauxite & Alumina Conference, 2013.
10. M. O' Driscoll, "The New World of China's Refractory Mineral Supply," in 61st International Colloquium on Refractories, Aachen, 2018.
11. C. Pascoal and V. C. Pandolfelli, "Bauxitas refratárias: Composição química, fases e propriedades - Parte I," Cerâmica, vol. 46, no. 298, pp. 76-89, 2000.
12. A. L. Pereira, M. A. Reis, L. L. H. C. Ferreira and P. M. Nakachima, "Brazilian refractory grade bauxite: a new alternative to refractories makers and users," Cerâmica, pp. 40-46, 2019.
13. J. Anggono, "Mullite Ceramics: Its Properties, Structure, and Synthesis," Journal Teknik Mesin, vol. 7, no. 1, pp. 1-10, 2005.
14. G. L. Lopes, "Processamento e Caracterização de Tialita a partir da Moagem de Alta Energia," Federal University of Alfenas, 2016.
15. G. R. Beardsmore and J. P. Cull, Crustal Heat Flow - A Guide to Measurement and Modelling, New York, 2001.
16. W. M. Haynes, CRC Handbook of Chemistry and Physics, Boca Raton: Taylor & Francis Group, 2017.
17. T. Huotari and I. Kukkonen, Thermal Expansion of Rocks: Literature Survey and Estimation of Thermal Expansion Coefficient for Olkiluoto Mica Gneiss, Posiva Oy, 2004.
18. K. Wefers, "Nomenclature, Preparation, and Properties of Aluminum Oxides, Oxide Hydroxides, and Trihydroxides," in Alumina Chemicals: science and technology handbook, 1990, pp. 13-22.
19. A. Caballero, J. Requena and S. Aza, "Refractory bauxites. How processing can improve high temperature mechanical properties," Ceramics International, vol. 12, no. 3, pp. 155-160, 1986.
20. C. I. Torres, N. M. Rendtorff, M. Cipollone, E. F. Aglietti and G. Suárez, "Comparative evaluation of properties of a clay based ceramic shaped via four techniques," Cerâmica, vol. 64, no. 370, pp. 176-182, 2018.
21. J. Eom, Y. Kim, C. B. Park and C. Wang, "Effect of forming methods on porosity and compressive strength of polysiloxane-derived porous silicon carbide ceramics," Journal of the Ceramic Society of Japan, vol. 120, no. 5, pp. 199-203, 2012.
22. A. B. Luz, J. A. Sampaio and S. C. A. França, Tratamento de Minérios, Rio de Janeiro: CETEM/MCT, 2010.
23. P. A. P. Martinez and W. F. J. Amorim, "Design of an Laboratory Polymer processing Extruder," 2019.
24. V. G. Oliveira, P. M. Nakachima, R. V. Fernandes, M. A. Reis, A. L. Pereira and L. L. H. C. Ferreira, "Improvement of the mechanical properties of green body bauxite briquettes through the addition of organic binders and methodologies for their evaluation," 63º Congresso Brasileiro de Cerâmica, 2019.
25. ISO 13503-2, Petroleum and natural gas industries - Completion fluids and materials — Part 2: Measurement of properties of proppants used in hydraulic fracturing and gravel-packing operations, 2006.
26. A. C. Larson and R. B. V. Dreele, General Structure Analysis System (GSAS), Los Alamos National Laboratory Report LAUR 86-748, 2004, p. 224.

27. B. H. Toby, "A Graphical user interface for GSAS," Journal of Applied Crystallography, pp. 210-221, 2001.
28. ABNT NBR 8592, "Grating dense refractory materials - Determination of bulk density - Method of test," Associação Brasileira de Normas Técnicas, 2012.
29. ABNT NBR 9642, "Refractory materials — Determination of hot modulus of rupture," Associação Brasileira de Normas Técnicas, 2012.
30. ABNT NBR 13320, "Refractory Materials - Determination of Fluidity of Conventional Castable and Castable of Free Flow," Associação Brasileira de Normas Técnicas, 2012.